scientific reports

Check for updates

OPEN

Characteristics of posterior precortical vitreous pockets visualized by swept-source OCT and *en face* OCT

Guangqi An[1,5], Min Zhang[2,5], Bo Lei[3], Xiaoyu Xin[3], Pei Liu[1], Yu Zhao[1], Haoxiang Chen[1], Xuemin Jin[1,4]✉ & Liping Du[1,4]✉

To determine the characteristics of posterior precortical vitreous pockets (PPVPs) and to observe vitreous changes in myopic eyes by swept-source optical coherence tomography (SS-OCT) and *en face* imaging in a cohort of the Chinese Han population. This was a cross-sectional study. Volunteers (235 participants, 374 eyes) received an SS-OCT examination. The heights and widths of the PPVPs were measured by SS-OCT. The area of the PPVPs was measured on *en face* images. The relationships between PPVP size and sex, age, axial length (AL) and spherical equivalent (SE) were evaluated. The mean width and height were 6711.64 ± 1241.87 μm and 662.47 ± 326.39 μm, respectively. The area of the PPVPs was 30.296 ± 9.114 mm^2. Boat-shaped, oval, and hook-shaped PPVPs were observed in 73.26%, 21.12%, and 5.62% of all eyes, respectively; 73.53% of all PPVPs had channels communicating with Cloquet's tubes. There was a significant difference in the PPVP width among the participates over and under 50 years old ($t = -2.508$, $P = 0.031$). Age had a positive correlation with the PPVP width ($r = 0.53$, $P = 0.001$). The PPVP height showed significant differences among the different myopia groups ($F = 3.618$, $P = 0.013$). SE had a negative correlation with the PPVP height ($r = -0.176$, $P = 0.001$). However, there were no correlations between the AL and the width, height or area of the PPVPs ($P = 0.117$; $P = 0.334$; $P = 0.057$, respectively). Age and myopia affect the size of PPVPs. SS-OCT greatly facilitates visualization of the complex structure of the vitreous.

Keywords Myopia, Posterior precortical vitreous pockets, Posterior vitreous detachment, Optical coherence tomography

The vitreous is a transparent gel-like structure with a volume of approximately 4 mL, 99% of which is water[1]. Thus, it is difficult to observe the vitreous by in vitro examinations[2].

In 1976, Worst[3] described the premacular bursa, which was observed by autopsy of a corpse's eyes. In 1990, Kishi et al.[4] discovered and described the posterior precortical vitreous pocket (PPVP), which is the same as the premacular bursa. The PPVP is a fluid cavity located in front of the macula. In fundus surgery, this structure can also be seen in eyes without posterior vitreous detachment (PVD)[5,6]. The anterior and posterior boundaries of PPVPs are the vitreous gel and posterior vitreous cortex, respectively[7].

With the development of imaging technology, researchers have used different types of optical coherence tomography (OCT) to observe PPVPs and have described their morphological characteristics and size[8]. Prior investigations revealed a septum between the Martegiani zone at the base of the vitreous tube (Cloquet's tube) and the PPVP[9]. Furthermore, previous studies have suggested that PPVPs are related to vitreoretinal interface diseases and that their changes may be relevant to the mechanisms underlying many vitreoretinal interface pathologies[6,14–18]. Swept-source OCT (SS-OCT) provides a clearer and more three-dimensional view of vitreoretinal structures, significantly increasing clarity in deep tissue imaging. SD-OCT uses a light source with a wavelength of 840–870 nm and a frequency-domain spectrometer as its detector. It has an axial resolution of 5–7 micrometers and a scanning speed ranging from 16,000 to 55,000 A-scans per second. In contrast, SS-OCT

[1]Department of Ophthalmology, The First Affiliated Hospital of Zhengzhou University, Zhengzhou, Henan, China. [2]Department of Ophthalmology, Zhengzhou People's Hospital, Zhengzhou, Henan, China. [3]Eye institute, Henan Academy of Innovations in Medical Science, Zhengzhou, Henan, China. [4]Institute of Fundus Diseases, Zhengzhou University, Zhengzhou, Henan, China. [5]These authors contributed equally: Guangqi An and Min Zhang. ✉email: 2740913223@qq.com; dulplab@live.cn

employs a 1050 nm Fourier domain mode-locked laser, achieving a scanning speed of 236,000 A-scans per second at a rate of 236 kHz, significantly increasing the scanning depth[10–13]. The application of SS-OCT in the observation of PPVP may provide an understanding of this structure.

However, previous studies had limited sample sizes from Japanese or Chinese populations with limited refractive levels or age[2,10,19–21]. Previous studies also lacked research on the relationship between the size of PPVPs and axial length (AL). Therefore, a large-sample study with a wider range of refractive levels and age is needed.

In this study, we performed SS-OCT on the eyes of 230 volunteers (374 eyes), observed the morphological characteristics of PPVPs and analyzed their relationship with sex, age, spherical equivalent (SE) and AL. We provided a detailed description of the morphological characteristics of PPVPs observed in healthy and myopic populations using SS-OCT technology.

Participants and methods

Participants

This was a cross-sectional study. A total of 250 volunteers (374 eyes) underwent SS-OCT imaging at the First Affiliated Hospital of Zhengzhou University from September 2021 to September 2022. All of the volunteers also underwent optometry checks, AL measurements, slit-lamp and fundoscopy examinations. The inclusion criteria were as follows: (1) age between 18 and 65 years. (2) PPVP could be observed by SS-OCT and the image quality was higher than 8.0, and (3) the best corrected visual acuity (BCVA) was 0.0 (log MAR). The exclusion criteria were as follows: (1) posterior vitreous detachment (PVD), vitreous-retinal disease, retinal detachment or tear, pathologic myopia, diabetic retinopathy, uveitis or other ocular pathologies affecting the vitreous; (2) previous vitrectomy or an ocular trauma history; or (3) inability to cooperate with an SS-OCT examination, e.g., because of conditions such as poor fixation.

This study was approved by the Ethics Committee of the First Affiliated Hospital of Zhengzhou University [No. 2022-KY-0512-001]. Based on the *Declaration of Helsinki*, we collected demographic information and clinical examination results after informed consent was obtained from the volunteers or their guardians. The clinical examination results included BCVA, SE, AL, and SS-OCT images. All basic data were recorded individually by two investigators. If the data provided by the two investigators differed, a third investigator would contact the volunteers to confirm the accurate data.

SS-OCT examination method and measurement of PPVP

Skilled ophthalmologists performed SS-OCT (VG100 or 200, Intalight, China) scans on each participant. Each participant underwent star line scanning, supplemented with multi-line scanning. Additionally, some participants underwent Angio or Cube scanning with a scan line length of 12 to 16 mm and a scan square of 12 mm × 12 mm. The depth of the scanning was 3 to 6 mm. The scanning laser wavelength was 1050 mm, and the scanning speed was 200,000 times/second. All the participants were seated, with their heads resting on a chin rest. To determine the presence of PPVPs and the vitreous, the operator manually focused on the front of the retina instead of autofocusing.

We adopted the "Enhance" function in the SS-OCT software to increase the brightness and contrast of the pattern to display the PPVPs better. To unify the standard, convenient positioning, we used B-Scan images of scan lines through the fovea and optic disc for subsequent analysis. To determine the size of PPVPs, the transverse longest meridians of the PPVPs served as their width, and the vertical line from the macular fovea to the vitreous gel interface served as the height of PPVPs (Fig. 1). Two junior ophthalmologists measured and recorded the size independently by manual measurements using the "Measuring ruler" function of the SS-OCT.

The en face images were reconstructed by the "en face" function of SS-OCT on vitreous image, which was based on 12 mm×12 mm Angio scanning. The areas of the PPVPs were measured by the two junior ophthalmologists using the "Measuring area" function of the SS-OCT.

A third ophthalmologist used the averaging method to calculate the data (widths and heights, areas of PPVPs). If there was a significant deviation between the two measurements, a senior ophthalmologist repeated the measurement to adjudicate.

Other ophthalmic examinations and grouping

Experienced optometrists tested the BCVA and SE. AL was measured using an IOL-Master 500 (Carl Zeiss, Germany). All participants underwent slit lamp and fundoscopy conducted by retina specialists to rule out fundus lesions.

Because 50 years of age is the peak age for PVD. According to age, we divided the participants into two groups: under 50 years old and 50 or above 50 years old.

The SE was calculated as a spherical mirror + 1/2 cylinder. According to the SE, we divided the eyes into four groups: nonmyopic group ($-0.25\ D \leq SE \leq +1.00\ D$) (Group A), low myopia group ($-3.00\ D \leq SE < -0.25\ D$) (Group B), moderate myopia group ($-6.00\ D < SE < -3.00\ D$) (Group C), and high myopia group ($SE \leq -6.00$) (Group D).

When discussing age, we acknowledged that including both eyes of the same subject could lead to non-independence of data. Therefore, in our analysis of age and PPVP size, we selected one eye of binocular participants to form a new sample using the random number method (encoding the right eye as 1 and the left eye as 2, and then randomly selecting one of the eyes). This approach ensures scientific statistical analysis and inter-group independence.

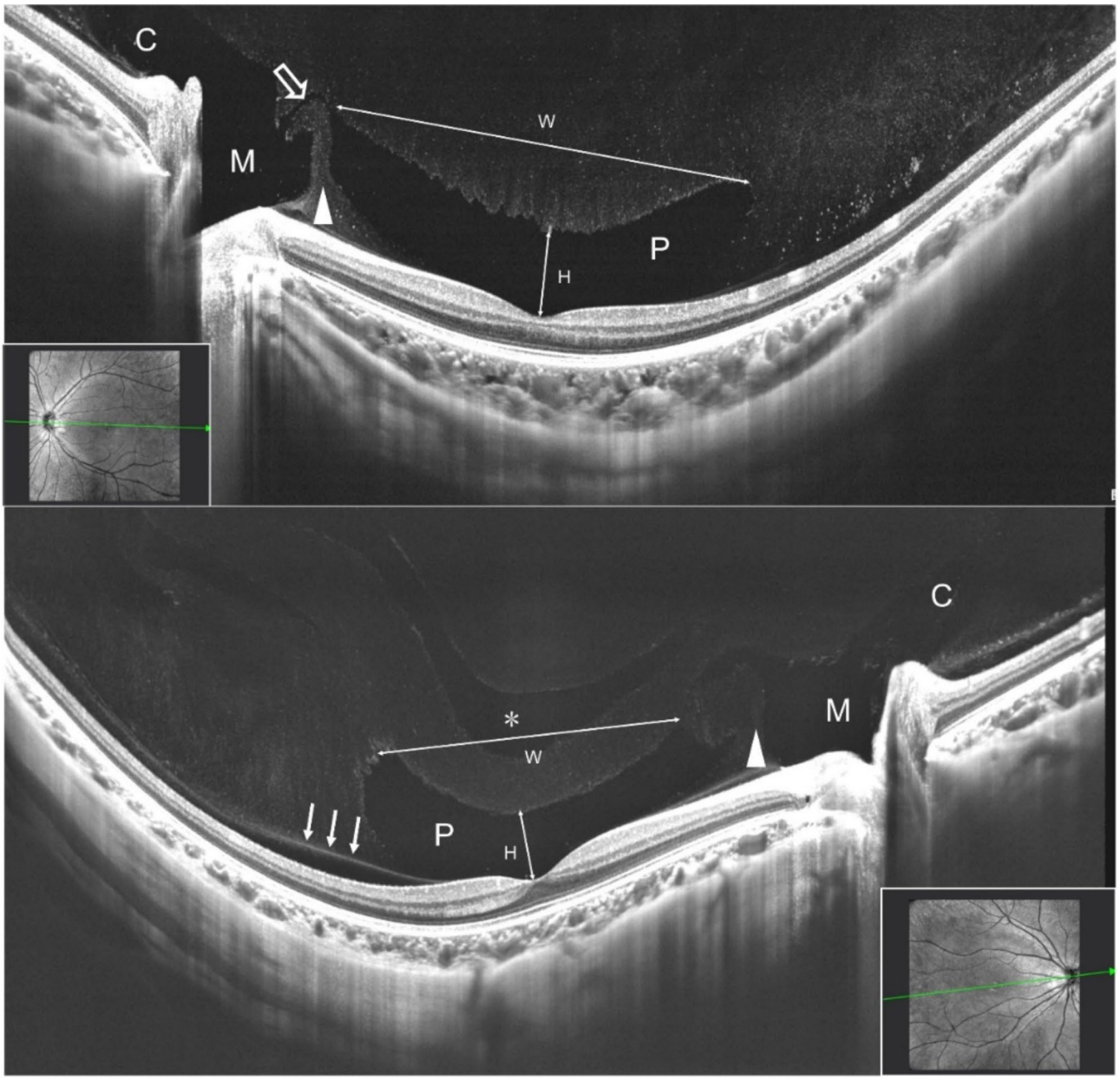

Fig. 1. B-Scan images from the left eye of a 22 years female which SE was −3.50D (above) and the right eye of a 26 yreas. female which SE was −4.25D (below). The measurement method of PPVPs, w: The width of PPVP; H: The height of PPVP; P: Low signal cavity showed the PPVP, macular anterior ship-type liquid cavity; C: low-signal tubular cavity showed the vitreous tube (Cloquet's tube), from the posterior pole of the lens to the remnant of the original vitreous tube in front of the optic disc; M: low signal cavity showed the Martegiani area, Cloquet's tube connecting the base of the optic disc; *: vitreous liquefaction cavity; White arrow head: A slightly higher signal diaphragm can be observed in the PPVP and Martegiani area, which named a septum; White hollow arrow: A channel connecting PPVP and Cloquet's tube on the septum; White arrow: Posterior vitreous detachment.

Statistical analysis

We used SPSS statistics 26.0 software (IBM Corp.; USA) for data analyses. The χ^2 test was used to analyze the categorical data, which are described using frequencies and percentages. The Kolmogorov–Smirnov test was performed to verify whether all the data sets were distributed normally. Normally distributed data are herein described as the mean and standard deviation, and ANOVA and *t*-test was used for comparisons. Pearson correlation analysis was used for the correlation analysis. A P value of < 0.05 was considered to indicate statistical significance.

Results

Demographics of participants

A total of 374 eyes of 230 participants were included in this study, including 83 males and 147 females. Eighty-six participants included one eye, and 144 participants included both eyes after review of the SS-OCT image. Their age was (25 ± 9.68) years, with a range of 8 to 63 years. The SE of all eyes was (− 3.44 ± 2.47) diopters (D) with a range of − 11.50 to + 1.00 D. The mean AL of all eyes was (25.04 ± 1.22) mm, with a range of 22.12 mm to 28.46 mm.

We used a random number method to obtain a sample of 230 eyes from 230 participants. This sample included 120 right eyes and 110 left eyes. Their SE was − 2.52 ± 0.93 D with a range of − 11.50 to + 1.00 D. The mean AL of all eyes was (24.98 ± 1.21) mm with a range of 22.12 mm to 28.46 mm. There was no statistically significant difference in the SE and AL of this sample compared to the total sample ($P = 0.229$, $P = 0.502$).

SS-OCT and enface findings of PPVPs

The width of the PPVPs was 3655.30 to11595.74 μm, and the mean width was 6711.64 ± 1241.87 μm. The height of the PPVPs was 64.8 to 2325.04 μm, and the mean height was 662.47 ± 326.39 μm.

Overall, the commonest PPVP shape in B scans through the fovea and the optic disc was the boat-shaped (73.26%) anterior macula. However, we also observed oval (21.12%) and hook-shaped (5.62%) PPVPs. The shapes of PPVPs are shown in Fig. 2. Among the 144 binocular participants, 118 (81.94%) had PPVPs of the same shape in both eyes.

We observed all B-scans to determine if the PPVPs communicated with the Martegiani area, as shown in Fig. 1 (white hollow arrow), where channels and septa existed. Of the 374 eyes, 275 (73.53%) eyes had this channel. Among the 144 binocular participants, 134 (93.06%) had the same situation in both eyes. Twenty-one of 43 (48.84%) junior participants, 153 of 162 (94.44%) young participants and 21 of 25 (84.00%) middle-aged participants had this channel.

Sixty participants (107 eyes) underwent 12 mm×12 mm Angio scanning, and en face images were obtained. There were dark round areas on en face images in 78 eyes (72.89%) of 41 participants (11 males and 30 females). The areas of PPVPs ranged from 17.729 to 60.621 mm^2, and the mean area was 30.296 ± 9.114 mm^2.The PPVP area was related to the PPVP width ($r = 0.485$, $P < 0.001$) and correlated with the PPVP height ($r = 0.819$, $P = 0.026$).

The relationship between sex, age and PPVP size

The age between males and females was not significantly different (t = -1.22, $P = 0.222$). Meanwhile, the width and height of the PPVPs were not significantly different in the different sexes ($t = 0.03$, $P = 0.979$; $t = 0.03$, $P = 0.979$). (Supplement Table 1). In 41 eyes of 41 participants with en face images, the areas of the PPVPs were 35.53 ± 11.424 mm^2 and 29.127 ± 7.693 mm^2 in males and females, respectively. The PPVPs significantly differed between the sexes ($t = 2.067$, $P = 0.045$).

We selected 39 nonmyopic eyes from 39 participants for analysis to rule out the effects of myopia. The SE and AL showed no significant differences between participates over and under 50 years old (t = − 1.144, $P = 0.260$; $t = 407$, $P = 0.686$). The PPVP width showed significant differences among between participates over and under

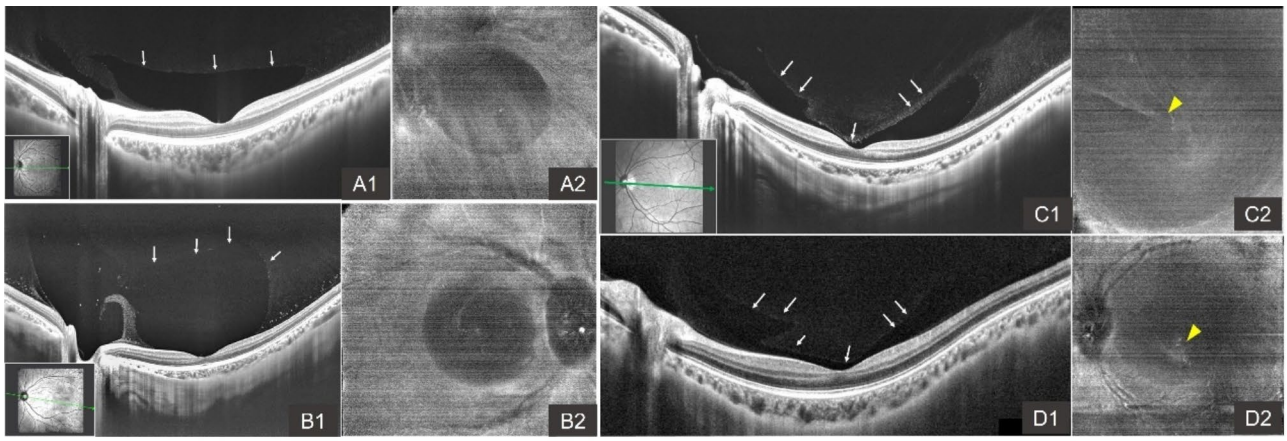

Fig. 2. A boat-shaped PPVP (A1, A2), An oval PPVP (B1, B2), and hook-shaped PPVPs (C1, C2 and D1, D2). A1 and A2 were SS-OCT B-Scan and en face OCT images from the left eye of a young female which SE was − 0.75D. This PPVP was boat-shaped, sharp at both ends. The anterior edge was vitreous gel, slightly upturned arc at both ends, posterior edge was posterior vitreous cortex. B1 and B2 were SS-OCT B-Scan and en face OCT images from the left eye of another young female which SE was − 3.75D. The anterior edge of this PPVP was flattened and rounded, and the curvature at both ends was rounded. C1, C2, D1 and D2 were SS-OCT B-Scan and *en face* OCT images from two young females. This PPVP was narrow and long, the vitreous body of the anterior edge is closer to the fovea, and the two ends were upturned and hooked. Yellow arrow heads showed the vitreous above the fovea.

50 years old ($t = -2.508$, $P=0.031$). Correlation analysis showed a positive correlation between age and PPVP width ($r=0.53$, $P=0.001$). The PPVP height showed no difference between participates over and under 50 years old ($t = -0.116$, $P=0.910$). (Supplement Table 2). Correlation analysis showed no correlation between age and PPVP height ($r=0.19$, $P=0.246$). All 58 participants with en face images were under 50 years old. There was negative correlation between age and PPVP area ($r = -0.37$, $P=0.019$).

The relationship between SE and PPVP size

We included 355 eyes of 217 participants under 50 years old for analysis to exclude the effect of age. The PPVP width showed no statistically significant differences among Group A, Group B, Group C and D ($F=1.463$, $P=0.224$) (Supplement Table 3). When we compared each group with all the remaining groups, there was no statistically significant differences (Supplement Table 4). We performed between-group comparisons, there was statistically significant differences between Group A and D ($P=0.039$) (Supplement Table 5). There was no correlation between the SE and the width of PPVPs (r = -0.026, $P=0.065$).

For height, there was a significant difference among the groups ($F=3.618$, $P=0.013$) (Supplement Table 3). When we compared each group with all the remaining groups, there were no statistically significant differences between B with other groups and D with other groups ($t = -2.60$, $P=0.01$; $t=2.884$, $P=0.004$) (Supplement Table 4). Furthermore, the *LSD-t* test indicated that there were differences in group B, C and D ($P=0.001$; $P=0.020$) (Supplement Table 5). There was correlation between the SE and the height of PPVPs ($r = -0.176$, $P=0.001$).

Among 190 eyes of the 58 participants with en face images, 9 eyes had high myopia, 53 eyes had moderate myopia, 28 eyes had low myopia, and 19 eyes had no myopia. The areas were 33.779 ± 9.790 mm^2, 32.165 ± 9.59 mm^2, 30.64 ± 8.19 mm^2, and 33.71 ± 9.83 mm^2. There were no significant differences among the four groups ($F=0.513$, $P=0.675$).

The relationship between AL and PPVP size

According to a previous study, AL is related to SE. This sample also fit this rule ($r = -0.737$, $P<0.001$). Therefore, we also investigated the correlation between the AL and the size of PPVPs. However, there was no correlation between the AL and the width, height or area of the PPVPs ($P=0.117$; $P=0.334$; $P=0.057$).

Discussion

In this study, we evaluated 374 eyes to observe different shapes of PPVPs and described their characteristics. We used more scientific statistical methods to group 374 eyes in detail, avoiding inter group bias. We observed more diverse morphologies of PPVPs than previous studies did. However, the majority of PPVPs were boat-shaped when the participants were seated, which was similar to the findings in previous studies[2,10,11,13,20]. A total of 81.94% of binocular participants had the same PPVP morphology in both eyes, which was consistent with previous studies[11,21]. In addition, we observed oval PPVPs and hook-shaped PPVPs, suggesting that the morphology of PPVPs was diverse. Our results showed that the vitreous is a complex structure that can be best observed by a combination of SS-OCT and 3D images based on en face technology. Longer OCT B-Scan lines (more than 12 mm) and larger OCT C-Scan squares (more than 12×12 mm) could show full posterior poles of the eyes. In contrast, 3D images are more intuitive, but there are problems such as a large data volume, which requires more accurate and faster algorithms. SS-OCT, including ultrawide-field SS-OCT (UWF SS-OCT), en face images and 3D images, is a better method to observe the structures of the posterior vitreous in normal and pathologic eyes than other OCT[7,22,23]. en face SS-OCT provides a new perspective for observing PPVPs.

Itakura et al.[11] observed that 93.1% of eyes in adults had a channel between the Martegiani area at the base of Cloquet's tube and the PPVP. However, Park et al.[21] reported that the channel was not observed in 3 to 4-year-old participants, while 50% of 11-year-old subjects exhibited the channel. A total of 44.48% of children between 8 and 18 and 93.04% of the adults in this study had channels. In total, 73.53% of the 374 eyes had channels. The Cloquet tube is a remnant of the original vitreous body, which emanates from the Martegiani area and connects to the posterior pole of the lens in the Berger area[12,13]. It was speculated that the liquid in PPVPs may be aqueous humor.

The mean PPVP width and height of 374 eyes in this study were 6711.64 ± 1241.87 μm and 662.47 ± 326.39 μm, respectively, which were smaller than those in previous studies. The sample in our study was younger, and the average height was similar to that in previous studies[11,24]. Park et al.[21] demonstrated that the PPVP width in children is smaller than that in adults, and that this width is proportional to age; She et al.[2] also obtained the same result. We also observed the following phenomenon: the width of the PPVPs differed in the different the participates over and under 50 years old ($t = -2.508$, $P=0.031$), but the height of the PPVPs exhibited no difference ($t=0.116$, $P=0.910$). The width of the PPVPs became larger with age ($r=0.526$, $P=0.001$).

There have been few studies on the relationship between PPVP size and SE. In this study, the PPVP height decreased in the low myopia group (659.25 ± 358.8) μm compared with the non-myopia group (659.25 ± 358.87) μm, and the PPVP height increased again as the diopter increased to moderate myopia (643.40 ± 325.10) μm and high myopia (821.88 ± 326.92) μm, which was the same finding as that by Itakura et al.[19]. However, this result was contrary to the conclusion reached by She et al.[2]. We also performed correlation analyses of AL and PPVP size and did not obtain positive results. We believe that with the decrease in SE, there may be more morphological changes in the eyeball that are not only stretched along the optical axis[25]. The changes might affect the morphology of PPVPs. However, the role and change in PPVPs need to be further studied by combining parameters such as eye morphology.

In conclusion, age and myopia affect the size of PPVPs. SS-OCT reveals the characteristics of PPVPs in vivo. UWF SS-OCT based on en face technology can provide more details of PPVPs, which will enhance our management of vitreoretinal disorders. This study provides essential data that can serve as a foundation for

future research in disease states, contributing to a better understanding of PPVPs in both health and disease. Future studies should consider including a wider range of vitreoretinal diseases to further elucidate the complex relationships between vitreous morphology and retinal health.

Data availability

The datasets used and/or analysed during the current study available from the corresponding author on reasonable request.

Received: 27 January 2024; Accepted: 26 September 2024
Published online: 10 October 2024

References

1. Spaide, R. F. et al. Imaging the vitreous with a novel boosted optical coherence tomography technique: vitreous degeneration and cisterns. *Retina*. **42** (8), 1433–1441. https://doi.org/10.1097/IAE.0000000000003474 (2022).
2. She, X. et al. Characteristics of posterior precortical vitreous pockets and Cloquet's canal in patients with myopia by optical coherence tomography. *Investig. Ophthalmol. Vis. Sci.***60** (14), 4882–4888. https://doi.org/10.1167/iovs.19-27426 (2019).
3. Worst, J. G. F. The bursa intravitrealis premacularis. *Dev. Ophthalmol.***7**, 275–279 (1976).
4. Kishi, S. & Shimizu, K. Posterior precortical vitreous pocket. *Arch. Ophthalmol.***108** (7), 979–982. https://doi.org/10.1001/archopht.1990.01070090081044 (1990).
5. Shimada, H. et al. Three-dimensional depiction of the vitreous pocket using triamcinolone acetonide. *Eur. J. Ophthalmol.***19** (6), 1102–1105. https://doi.org/10.1177/112067210901900638 (2009).
6. Fine, H. F. & Spaide, R. F. Visualization of the posterior precortical vitreous pocket in vivo with triamcinolone. *Arch. Ophthalmol.***124** (11), 1663. https://doi.org/10.1001/archopht.124.11.1663 (2006).
7. Ohno-Matsui, K. et al. Determining posterior vitreous structure by analysis of images obtained by AI-based 3D segmentation and ultrawidefield optical coherence tomography. *Br. J. Ophthalmol.*https://doi.org/10.1136/bjophthalmol-2021-320131 (2021).
8. Kim, Y. C. et al. Enhanced high-density line spectral-domain Optical Coherence Tomography Imaging of the Vitreoretinal Interface: description of selected Cases. *Semin Ophthalmol.***31** (6), 559–566. https://doi.org/10.3109/08820538.2015.1009560 (2016).
9. Gal-Or, O. et al. In vivo imaging of the fibrillar architecture of the posterior vitreous and its relationship to the premacular bursa, Cloquet's canal, prevascular vitreous fissures, and cisterns. *Graefes Arch. Clin. Exp. Ophthalmol.***257** (4), 709–714. https://doi.org/10.1007/s00417-018-04221-x (2019).
10. Li, D. et al. Posterior precortical vitreous pockets and connecting channels in children on swept-source optical coherence tomography. *Investig. Ophthalmol. Vis. Sci.***55** (4), 2412–2416. https://doi.org/10.1167/iovs.14-13967 (2014).
11. Itakura, H. et al. En face imaging of posterior precortical vitreous pockets using swept-source optical coherence tomography. *Investig. Ophthalmol. Vis. Sci.***56** (5), 2898–2900. https://doi.org/10.1167/iovs.15-16451 (2015).
12. Kishi, S. Impact of swept source optical coherence tomography on ophthalmology. *Taiwan. J. Ophthalmol.***6** (2), 58–68. https://doi.org/10.1016/j.tjo.2015.09.002 (2016).
13. Schaal, K. B. et al. The premacular bursa's shape revealed in vivo by swept-source optical coherence tomography. *Ophthalmology*. **121** (5), 1020–1028. https://doi.org/10.1016/j.ophtha.2013.11.030 (2014).
14. Kishi, S. & Shimizu, K. Clinical manifestations of posterior precortical vitreous pocket in proliferative diabetic retinopathy. *Ophthalmology*. **100** (2), 225–229. https://doi.org/10.1016/s0161-6420(93)31666-0 (1993).
15. Itakura, H. & Kishi, S. Evolution of vitreomacular detachment in healthy subjects. *JAMA Ophthalmol.***131** (10), 1348–1352. https://doi.org/10.1001/jamaophthalmol.2013.4578 (2013).
16. Sato, T. et al. Modified technique for inducing posterior vitreous detachment through the posterior precortical vitreous pocket during microincision vitreous surgery with a wide-angle viewing system. *Ophthalmologica*. **230** (2), 76–80. https://doi.org/10.1159/000351655 (2013).
17. Hanai, K. et al. Microsurgical observation of the posterior vitreous in patients with vitreous hemorrhage caused by Terson syndrome. *Am. J. Ophthalmol. Case Rep.***17**, 100613. https://doi.org/10.1016/j.ajoc.2020.100613 (2020).
18. Spaide, R. F. Measurement of the posterior precortical vitreous pocket in fellow eyes with posterior vitreous detachment and macular holes. *Retina*. **23** (4), 481–485. https://doi.org/10.1097/00006982-200308000-00006 (2003).
19. Itakura, H. et al. Vitreous changes in high myopia observed by swept-source optical coherence tomography. *Investig. Ophthalmol. Vis. Sci.***55** (3), 1447–1452. https://doi.org/10.1167/iovs.13-13496 (2014).
20. Itakura, H. et al. Observation of posterior precortical vitreous pocket using swept-source optical coherence tomography. *Investig. Ophthalmol. Vis. Sci.***54** (5), 3102–3107. https://doi.org/10.1167/iovs.13-11769 (2013).
21. Park, K. A. & Oh, S. Y. Posterior precortical vitreous pocket in children. *Curr. Eye Res.***40** (10), 1034–1039. https://doi.org/10.1136/bjophthalmol-2019-314591 (2015).
22. Mitsch, C. et al. Systematic ultrastructural comparison of swept-source and full-depth spectral domain optical coherence tomography imaging of diabetic macular oedema. *Br. J. Ophthalmol.***104** (6), 868–873 (2020).
23. Leong, B. C. S. et al. OCT en Face Analysis of the posterior vitreous reveals Topographic relationships among Premacular Bursa, Prevascular fissures, and Cisterns. *Ophthalmol. Retina*. **4** (1), 84–89. https://doi.org/10.1016/j.oret.2019.09.002 (2020).
24. Shimada, H. et al. Depiction of the vitreous pocket by optical coherence tomography. *Int. Ophthalmol.***31** (1), 51–53. https://doi.org/10.1007/s10792-010-9398-4 (2011).
25. Sankaridurg, P. et al. IMI Impact of Myopia. *Investig. Ophthalmol. Vis. Sci.***62** (5), 2. https://doi.org/10.1167/iovs.62.5.2 (2021).
26. An, G. et al. Characteristics of posterior precortical vitreous pockets visualized by swept-source OCT and en face OCT. Research Square. https://doi.org/10.21203/rs.3.rs-3215580/v1.

Acknowledgements

I would like to acknowledge Dr. Wenna Gao in The First Affiliated Hospital of Zhengzhou University, Dr. Xiaohong Guo, Dr. Qingge Guo, and Dr. Changgeng Liu in Henan Eye Hospital & Henan Eye Institute, for their guidance during this research. I would like to thank all the volunteers in this study. This manuscript was previously submitted as a pre-print at Research Square with the link "https://www.researchsquare.com/article/rs-3215580/v1"[26].

Author contributions

Conception and design: Guangqi An, Min Zhang, Liping Du. Data collection: Guangqi An, Min Zhang, Xiaoyu Xin, Pei Liu, Yu Zhao, Haoxiang Chen. Analysis and interpretation: Guangqi An, Min Zhang, Xiaoyu Xin, Pei

Liu, Yu Zhao, Haoxiang Chen. Obtained funding: Liping Du, Xuemin Jin. Overall responsibility: Guangqi An, Min Zhang, Bo Lei, Liping Du, Xuemin Jin.

Funding
This work was supported by National Natural Science Foundation of China [81970792 and 82171040] and Medical Science and Technology Project of Health Commission of Henan Province [YXKC2020026].

Declarations

Competing interests
The authors declare no competing interests.

Additional information
Supplementary Information The online version contains supplementary material available at https://doi.org/10.1038/s41598-024-74461-x.

Correspondence and requests for materials should be addressed to X.J. or L.D.

Reprints and permissions information is available at www.nature.com/reprints.

Publisher's note Springer Nature remains neutral with regard to jurisdictional claims in published maps and institutional affiliations.